PAPER

Shear thickening fluid with tunable structural colors

IOP Publishing Smart Materials and Structures
Smart Mater. Struct. **27** (2018) 095012 (11pp) https://doi.org/10.1088/1361-665X/aad587

Shear thickening fluid with tunable structural colors

Mei Liu[1], Wanquan Jian[1,3], Sheng Wang[1], Shouhu Xuan[2], Linfeng Bai[1], Min Sang[1] and Xinglong Gong[2,3]

[1] Department of Chemistry, Collaborative Innovation Center of Suzhou Nano Science and Technology, University of Science and Technology of China (USTC), Hefei 230026, People's Republic of China
[2] CAS Key Laboratory of Mechanical Behavior and Design of Materials, Department of Modern Mechanics, USTC, Hefei 230027, People's Republic of China

E-mail: jiangwq@ustc.edu.cn and gongxl@ustc.edu.cn

Received 16 May 2018, revised 16 July 2018
Accepted for publication 24 July 2018
Published 6 August 2018

Abstract

We report a kind of shear thickening fluid (STF) which exhibits non-iridescent structural colors (defined as colorful shear thickening fluid, c-STF). The color of the c-STF can be tuned in a whole visible light range via changing the particle size, the filling fraction and temperature. The color of this c-STF is characterized by reflection and transmission spectrum and the inner structure was observed via confocal microscope. The relationship between the structure transitions, color, and rheological properties are systematically investigate. The measurements show that the occurrence of photonic band gap is responded for the short-range geometric order. The semitransparent colorful STF create the possibility to observe the transition of inner structure in shear thickening (ST) phenomenon, which will attribute to further study the mechanism of ST. And the tuned colors also extend the potential applications such as full-color displays with a wide viewing angle and color-tunable soft armor.

Supplementary material for this article is available online

Keywords: shear thickening fluid, tunable structural color, short-range order, rheological properties, mechanism

(Some figures may appear in colour only in the online journal)

1. Introduction

Shear thickening fluid (STF) is a kind of smart material by dispersing micro-and nano- particles into the carrier fluids. Its viscosity sharply increases when the shear rate reaches to the critical value and can exhibit the transformation from a liquid state to a solid state. This behavior has a good reversibility that the viscosity restores to initial state quickly when the applied stress is relieved [1–4]. Based on the unique shear thickening (ST) effect, a wide array of applications are developed, such as dampers, 'liquid' armor, impact absorbers, control devices, sports shoe cushioning, rotary speed limiters, etc [5–9]. Particularly, among the body protective applications, STF treated fabrics are researched extensively in recent years [10–13]. Selim Gürgen *et al* studied the effect of silicon carbide additives on the stab resistance of STF treated fabrics [10]. Animesh Laha *et al* improved the impact resistance of p-aramid fabrics via adding silica-halloysite nanotubes into STF [11].

STF is composed of the suspended phase, the solvent, and the additive, in which the suspended phase is one of the most important factors that affects rheological properties of the STF. As far as we know, there are three kinds of particles for STF. The first kind studied is inorganic particles such as silica [14, 15], titania [16, 17], calcium carbonate [18, 19] alumina [20] and barium sulfate precipitated [21]. The second kind is deformable particles such as starch particles [22], blood cells [4]. The last kind is man-made particles such as polyvinylchloride (PVC), poly (styrene–acrylonitrile) (PS–AN) [4], polymethylmethacrylate (PMMA) [23], poly

[3] Author to whom any correspondence should be addressed.

(styrene–ethyl acrylate) (PS–EA) [24], carbon nanofibers [25]. Additionally, various additives were added into STF to improve the rheological properties in order to apply to more application fields [26–28]. Silim Gürgen proposed a novel concept of multi-phase STFs, which were mixtures of single-phase STFs and various kinds of additives such as metal particles, ceramic particles and carbon nanotubes. In their concept, the additives were regarded as a suspended phase, which affect the rheological properties of STFs through varying the interactions between additives and another suspended phase.

Various mechanisms have been developed to explain the ST behavior such as order–disorder transition [2, 3, 29], dilatancy [30] and hydrocluster [31]. The most widely accepted is hydrocluster mechanism, in which hydrodynamic lubrication forces completely overcome the inter-particle repulsive forces at high shear rate, and this results in shear induced self-assembled hydroclusters that increase the viscosity. Many experimental methods, such as small angle neutron scattering experiments [32, 33], rheo-optical experiments [34] and the combination fast confocal microscopy with simultaneous force measurements, are developed to investigate the mechanism for a long time [35]. However, direct observation of the transient response of ST behavior when subjected sudden impact is always one of the challenges for developing the ST mechanism [36–39]. The colors of almost all kinds of the STFs are cloudy and opaque by far [1]. Therefore, we hope to develop a kind of semitransparent colorful STF to observe ST phenomenon and expect to open a new way to study ST mechanism.

Photonic crystal is one of the most representative colored materials exhibiting iridescent structural color due to its long-range order periodic microstructure. However, this kind of color changes dramatically depending on the angle of observation [40, 41]. There is also a different class of PBG material in nature, 'quasi-amorphous photonic materials', with only short-range order on the length scale of optical wavelength but without long-range order, exhibits non-iridescent structural color that have little angle-dependence [42–47], which is often observed in certain animals and insects due to their quasi-amorphous nanostructures present in their colored epidermises [48–50]. The structural color of these materials originates from wavelength-specific constructive interference in the visible region [51]. It was reported that condensed gel particle suspensions also display non-iridescent structural color [52]. However, non-iridescent structural color in the ST suspension has not been reported till now. Although various kinds of solid particles have been applied for STF, few of them presented the non-iridescent structural color due to the different refractive index between the particles and the carrying fluid.

SiO_2 nanospheres can be well synthesized through Stöber hydrolysis method, [53–56] which is the most used material to prepared STF and is also a kind of photonic crystal material. However, SiO_2-based STF is white and opaque for a long time due some different reasons. Firstly, the polydispersity index (PDI) of SiO_2 nanospheres is not small enough. Secondly, the surface chemistry properties of SiO_2 are different due to different washing method. Thirdly, the refractive indexes of the SiO_2 and carrier fluid are different. In this work, the PDI of SiO_2 nanospheres is within 5% via strictly controlling the experiment conditions. The SiO_2 is cleaned only with ethyl alcohol and the surface is rich of alcoholic hydroxyl group, which has good compatibility with PEG 200. Finally, the refractive index of SiO_2 and PEG 200 is almost the same. For these reasons, semitransparent and colorful STF was obtained.

By employing the visual spectrum investigation, we show that the structural colors are originated from the indirect reflection for the inner structure. A preliminary relationship is established among the structural color, temperature and the rheological properties, which mean that the color of STF has the prospect can be applied in practical applications. Direct observation of the transition from fluid to solid when subjected impacts in STF is obtained, which may proposed a new way for detecting the structure evolution mechanism of the ST phenomenon. The color of the c-STF is also dependent on the temperature, which indicates it possesses high potential in multifunctional soft armor-defending materials with the function of changing color under different conditions.

2. Experiment section

2.1. Materials

Tetraethylorthosilicate (TEOS, chemical pure), ethanol (analytical reagent), ammonium hydroxide ($NH_3 \cdot H_2O$, 25%–28%, analytical reagent) and poly (ethylene glycol) 200 (PEG 200, analytical reagent) were all purchased from Sinopharm Chemical Reagent Co. All chemicals were used directly as received without further treatment. Re-distilled water was used in this work.

2.2. The preparation of the c-STF

Firstly, monodisperse SiO_2 nanospheres with different diameters were synthesized using the modified Stöber method. Then, a certain amount of SiO_2 nanospheres were added into PEG 200 and the mixture was mixed in a ball crusher to obtain a homogeneous dispersion. The final product was collected after 24 h when no large-scale aggregation was found in the suspension. The obtained c-STF was sealed in a vial before use.

2.3. Rheological measurements and visual spectrum characterization

The rheological properties of the STF were measured by using the rheometer (Physical, MCR301, Anton Paar) at 25 °C with cone-plate having a cone angle of 2° and a diameter of 25 mm. The rheological properties of each sample were measured under static loading conditions. The steady-shear tests were conducted with a gap size of 0.05 mm. In order to remove loading effects, a pre-shear of $1\ s^{-1}$ was applied for 60 s before collecting the experimental data. The reflection spectra of the suspensions (25 °C) were measured

using a UV–visible spectrometer (SolidSpec- 3700 DUV) with a 60 mm diameter integrating sphere and the transmission spectra of sample in a quartz glass cell with a 4 mm light path length. Digital optical micrographs were taken by a digital camera (Sony Exmor RS IMX230) and high-speed video camera (Phantom V2512). The samples were kept at 25 °C when taking photographs unless otherwise noted.

2.4. Characterization

The particle size and macroscopic features were determined by a field emission scanning electron microscope (20 kV, JEOL JSM-6700F SEM). The thickness of the shell was observed by a transmission electron microscopy (TEM, JEM-2011) with an accelerating voltage of 200 kV. Confocal microscopic image was observed by laser scanning Confocal microscopy (Leica DMi8).

3. Results and discussion

3.1. Characteristic structural colors of c-STF

To obtain the non-iridescent color, the PDI of SiO_2 nanospheres should be within 5%. The monodisperse SiO_2 nanospheres with different sizes are prepared by Stöber hydrolysis method. The different sizes are prepared through strictly controlling the ratios of reactants and reaction temperatures. Figure 1 shows the TEM, SEM images and size distributions of the monodisperse SiO_2 nanospheres with different diameters. The polydispersity is less than 5% determined by the attachment (DigitalMicrograph) of TEM, which means that the obtained SiO_2 nanospheres are also suitable for fabricate iridescent color photonic materials. By increasing the concentration of the TEOS precursor, the diameter of the SiO_2 nanospheres can be tuned from 200 to 350 nm.

C-STFs are prepared by dispersing monodisperse SiO_2 nanospheres in PEG200 through ball-milling process. Figure 2(A) shows photographs of prepared STFs of SiO_2 particles with diameter of 265 nm (a), 220 nm (b), 335 nm (c), 310 nm (d) and 300 nm (e) displaying pink, orange-yellow, green, blue, and purples, respectively, almost covering the whole visible light spectrum scope. The volume fraction of the dispersed phase of five kind c-STFs is kept as a constant (58%). Figure 2(B) is the corresponding reflection spectra (a)–(e) of the five kind c-STFs (a)–(e) of figure 2(A), the peak positions of the spectra are 639 nm, 583 nm, 528 nm, 458 nm, 420 nm, respectively, which is well consistent with the displaying color. In conclusion, the color change over the entire visible range and it can be precisely controlled by adjusting the particle size.

The color of c-STFs also can be controlled by adjusting the volume fractions. Figures 3(a) and (b) are transmission and reflection spectra of c-STFs of 265 nm silica (the size of particle is kept in constant), the volume fractions are 58%, 47%, 37.2%, 28.3% and 20.2%, respectively. The reflection spectra show that there is a red shift of the color when the volume fractions decrease. Moreover, the colloid systems do not contain any chromophores capable of absorbing visible light and the observed colors are consequence of the structural colors, which is further confirmed by results of transmission and reflection spectroscopy. The transmission spectra (figure 3(a)) exhibit shoulder-shape changes with certain inflection points at wavelength λ_s, such as the volume fraction are 58%, 47%, and 37.2%, which corresponding to the maximum wavelength of the refection peaks, respectively (figure 3(b)). The λ_s of c-STFs with the volume fractions of 28.3% and 20.2% disappears, maybe due to the disappearances of the reflection wavelengths over 700 nm. It is reported that the shoulder-shape peak of the samples is attributed to the combination of the 'incoherent' and 'coherent' scatterings in the short-range ordered structures, and the lack of long-range order leads the incoherent scatterings, which must be resulted from Rayleigh and Mie scatterings [47, 52, 57–59].

According to the PBG of ordered structures, the band gap of the amorphous photonic structures is related to the distance between particles, the filling fraction and the refractive index of the material. It is inferred that the center position of the reflection peak position will be at

$$\lambda \propto Dn_{\text{eff}}, \tag{1}$$

$$n_{\text{eff}}^2 = fn_{\text{SiO}_2}^2 + (1-f)n_{\text{PEG200}}^2, \tag{2}$$

where λ refers to the wavelength of reflection peak and D refers to the distance between particles. n_{eff} is the effective refractive index of the condensed colloid fluid, f is the filling fraction of SiO_2 particles n_{SiO_2} and n_{PEG200} refer to the refractive indices of SiO_2 and PEG 200, respectively [60].

It is obvious that the distance between particles (D) becomes larger with the decrement of volume fraction in condensed colloid fluid. The refractive indices of SiO_2 and PEG200 are almost the same, so n_{eff} is held constant. It can be inferred that the wavelength of the center position of the reflection peak (λ) will become larger by equations (1) and (2). In fact, the reflection spectrum of figure 3(b) indicates that the wavelength of the c-STF has a red shift when the volume fraction of particles decreases, which is coincident with above deduction.

Figure 4(A) is the photograph of photonic crystal fabricated by the evaporation deposition from the monodisperse SiO_2 nanospheres (265 nm) suspension, which exhibits brilliant green color. At the same time, the condensed colloid fluid of figure 4(B) is pink fabricated by the same particles. The structural color is well kept when the suspension is flowing, which indicates that a common PBG still exists in these amorphous-like structures when the average distance between particles is relatively constant though there is no long-range periodic structure. More interesting, the color observed from different surface of cuvette is different as shown in figure 4(C). The surface 'a' of cuvette is perpendicular to the light source direction, which exhibiting pink color. The surface 'b' is parallel to the light direction displaying green color. A possible reason is that the color of surface 'a' mainly comes from wavelength-specific constructive interference, while surface 'b' mainly comes from

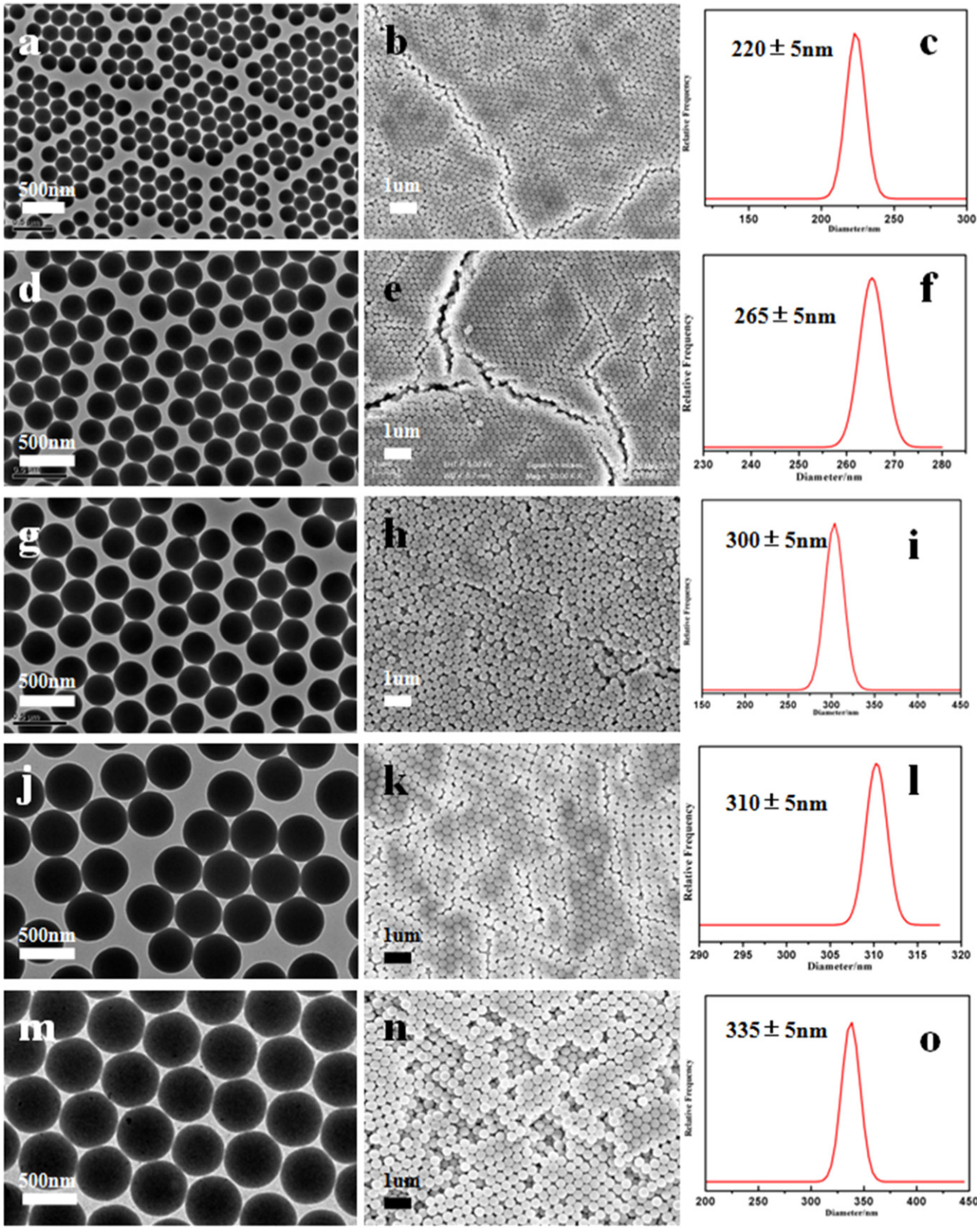

Figure 1. TEM (a), (d), (g), (j), (m), SEM (b), (e), (h), (k), (n) images and the size distributions (c), (f), (i), (l), (o) of SiO_2 with different diameters. The mean diameters of the five groups are 220 ± 5 nm (a)–(c), 265 ± 5 nm (d)–(f), 300 ± 5 nm (g)–(i), 310 ± 5 nm (j)–(l), 335 ± 5 nm (m)–(o).

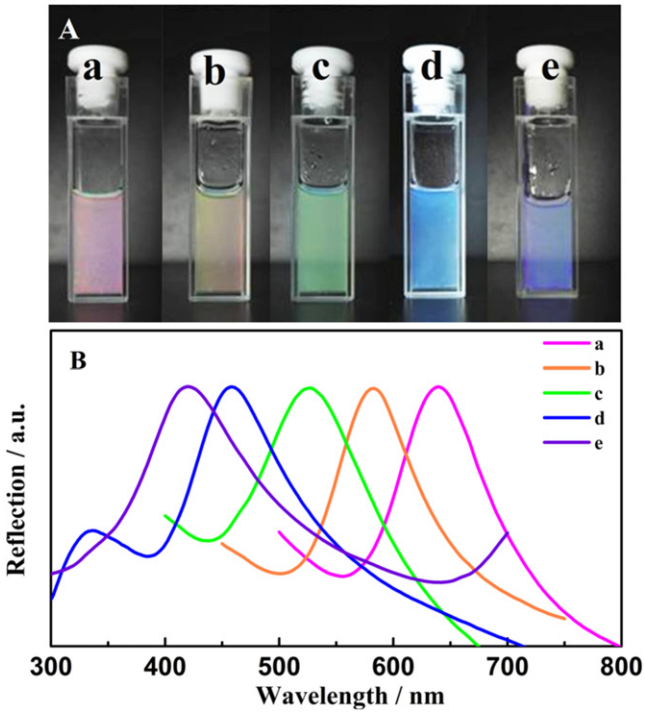

Figure 2. (A) Photographs of c-STFs with different structural colors. (B) Reflection spectra of c-STFs. The experiment temperature is controlled at 25 °C.

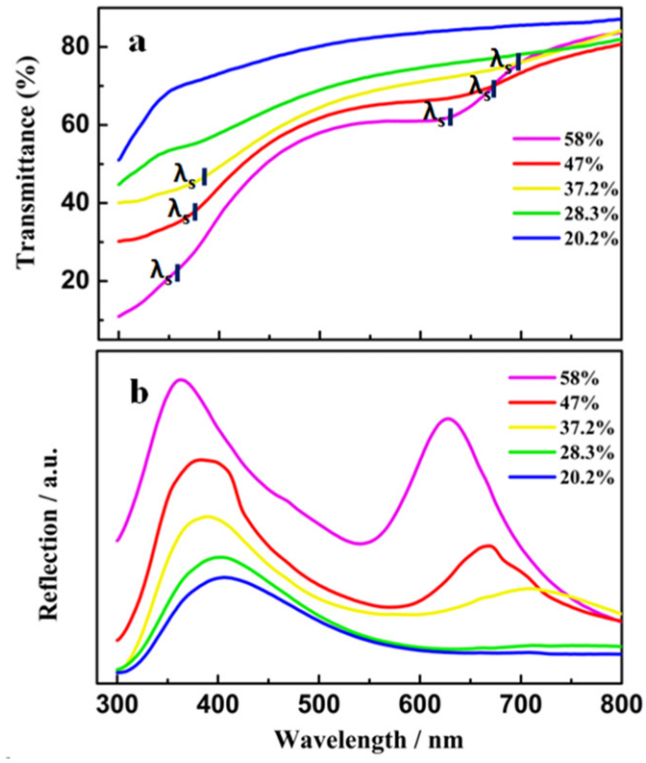

Figure 3. Transmission (a) and reflection spectra (b) of the suspensions with series volume fractions.

diffused light. However, the accurate principles of optics need to be further studied.

Figure 4(D) is the laser scanning confocal micrograph of suspension containing 20.2% (φ) silica content. From the

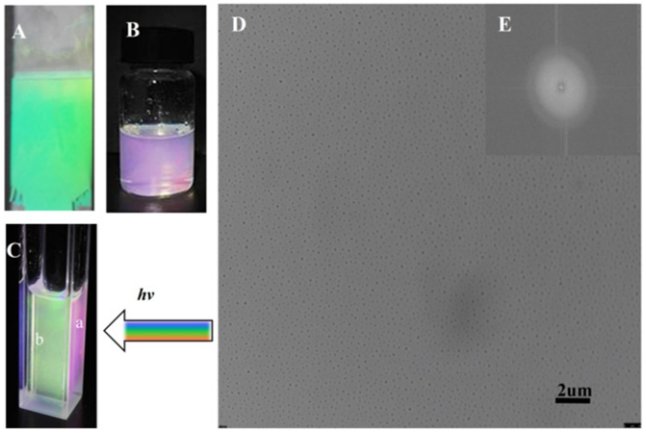

Figure 4. (A) Photonic crystal of SiO_2 on a glass slide with a mean diameter of 265 nm prepared by evaporation self-assemble method. (B) The photograph of p-STF of SiO_2 with a mean diameter of 265 nm. (C) The photograph of the varied color of pink p-STF observed from different angle paralleling or perpendicular to the lighting direction. (D) Confocal micrograph of suspension containing 20.2% (φ) silica content. (E) The image of two-dimension Fourier transform of the confocal micrograph.

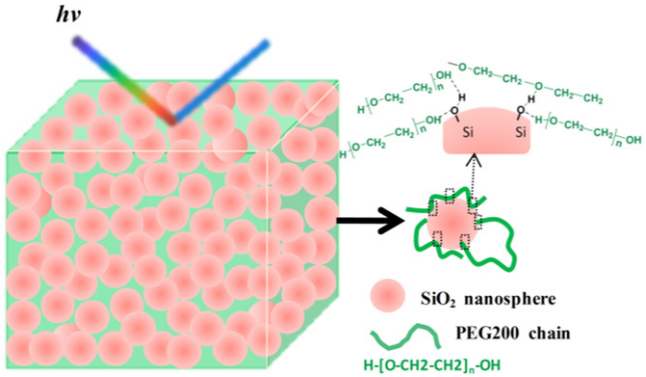

Figure 5. Illustration of the quasi-amorphous photonic structure of the c-STF and the way of displaying structural color and the right illustration is the interaction between SiO_2 nanospheres and PEG 200.

images, we can observe that the spatial periodicity exhibits a short-range order. The ring-shaped two-dimension Fourier transform (figure 4(E)) indicates that the particles are not fully randomly distributed but periodic of spatial variation in the refractive index in short-range. Furthermore, the circular ring shows that the periodicity of spatial variation in the refractive index is equivalent in all directions, which accounts for the angle-independent optical properties [57]. From the image of lower concentration suspension, we can deduce that the spatial periodicity also shows a short-range order at higher silica concentration.

Through characterizing optical properties, we further study the coloring mechanism in this colloidal photonic material. Inspired by the structure of colorful feather of birds, we find that the coloring mechanism in c-STF is similar to the mechanism in feather barbs of many bird species [61]. Figure 5 is the illustration of the quasi-amorphous photonic structure of the c-STF and the way of displaying structural

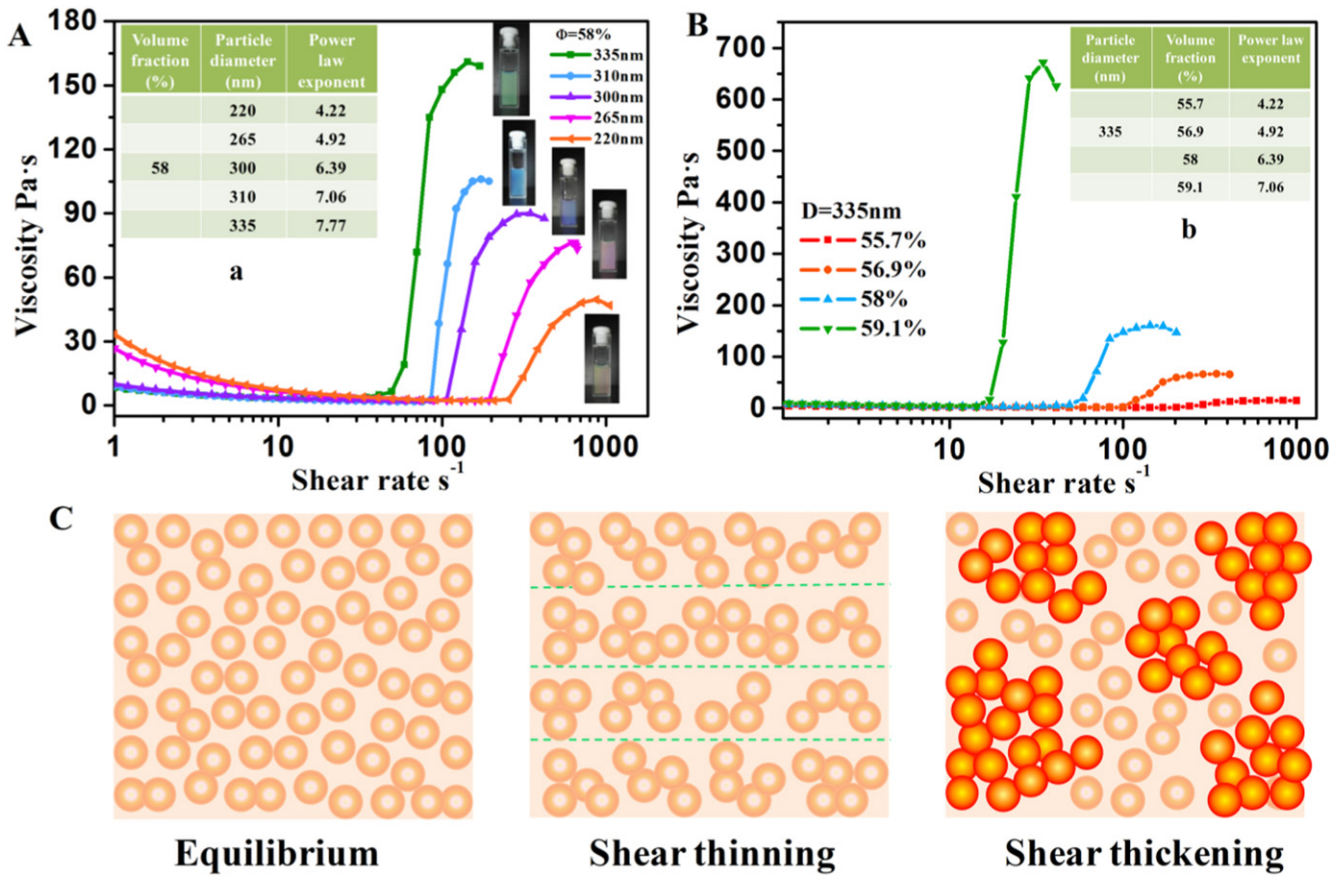

Figure 6. (A) The curve of viscosity versus shear rate for c-STFs of SiO_2 nanospheres with different diameters at the same volume fraction (58%). The inset table (a) shows power law exponents of c-STFs with different particle diameters while keeping the volume fraction a constant (58%). (B) The curve of viscosity versus shear rate for c-STF at a series of volume fractions when the particle size is constant (the average diameter of SiO_2 nanospheres is about 335 nm). The inset table (b) shows power law exponents of c-STF with different volume fractions when the particle size is constant. (C) The illustration of the change in microstructure of the colloid dispersion that explains the transitions from equilibrium to shear thinning and shear thickening.

color. The structure of nanospheres in colloid suspension always exhibits short-range order rather than long-range order. The intermolecular interactions between the surface of SiO_2 nanospheres and PEG 200 chains keep the condensed system relatively stable.

Tight-binding model is an explanation usually used in electronic band gap existed in semiconductors, which has been extended to photonic systems and indicating that PBG can also be formed without lattice periodicity or long-range order [62, 63]. Furthermore, Edagawa *et al* numerically showed that short-range order is the origin of the formation of PBG in photonic amorphous structures [45]. Due to the PBG of the photonic crystal is anisotropic, the iridescence color changes with angle variation, which limited the application in some areas requiring angle-independent structural color. Concerning this aspect, photonic quasi-amorphous materials with short-range order are completely isotropic and the PBG is independent of the incident light angle, which makes up the defects in photonic materials. In conclusion, our result is a new experimental candidate in exploring the exact mechanism of the PBG in the photonic amorphous structures as well as extract out the design principles of such amorphous structure.

3.2. The rheological properties of c-STF

Figure 6(A) shows the static rheological properties of c-STFs. Keeping the volume fraction as constant (58%), when the diameters of the particles are 335 nm, 310 nm, 300 nm, 265 nm and 220 nm, the initial viscosities are 8.2 Pa s, 8.9 Pa s, 10 Pa s, 26.7 Pa s, 33.4 Pa s and the critical shear rates are 49.2 s^{-1}, 85.5 s^{-1}, 107.4 s^{-1}, 192.9 s^{-1}, 255.4 s^{-1} respectively. At the same time, the maximum viscosities are 161 Pa s, 106 Pa s, 90 Pa s, 76.5 Pa s, 49.6 Pa s, respectively. Clearly, the initial viscosity and the critical shear rate increase with the decreasing of particle diameter. And the maximum viscosities decrease with the particle diameter decreasing. In conclusion, ST is moved to much higher shear rates with a reduction in particle size, which is in accord with the previous research results [4]. Additionally, five kinds of c-STFs prepared by SiO_2 with different diameters not only exhibit different rheological properties, but also show completely different color. The corresponding photographs of c-STFs with different colors are inserted in figure 6(A).

The rheological properties of c-STF are also controlled by changing the volume fraction of the dispersed phase. Figure 6(B) shows the rheological properties of c-STF with

different volume fractions. The volume fractions are 55.7%, 56.9%, 58%, 59.1%, corresponding shear rates are the 208.1 s^{-1}, 101.5 s^{-1}, 48.6 s^{-1}, 14 s^{-1} and the maximum viscosities are 14.5 Pa s, 70.6 Pa s, 162.5 Pa s, 672.9 Pa s, respectively. The critical shear rates decrease and the maximum viscosities increase with the increasing of volume fraction. It indicates that the ST become more intense with the increasing of the volume fraction of dispersed phase. However , the increase of intense in ST is not proportional to the increase volume fraction of dispersed phase. (Relevant explanation is in ESI.) For example, when the volume fractions vary from 55.7% to 59.1% (about 1 time), the maximum viscosities vary from 14.5 Pa s to 672.9 Pa s (46 times).

The color of c-STFs varies with the changes of particle size and the volume fraction, which are also the critical parameters of controlling the rheological properties of STF. The results enlighten us that there is the prospect that the rheological properties of c-STFs could be predicted via observing its color. By controlling their structural color, c-STFs with specific rheological properties can be obtained.

In order to further analyze and demonstrate the influence of volume fraction and particle size on shear thickening effect, we used power law exponents which are fitted from the steady-shear curves to characterize the degree of shear thickening. The relationship between viscosity and shear rate can be fitted by a power law function, as equation (5)

$$\eta = K^{*}\dot{\gamma}^{n-1}. \tag{5}$$

In this function, η is viscosity of suspensions, n is the power law exponent indicating the shear thickening effects, and K is the consistency index. The tables of power law exponents of n are inserted in figures 6(A) and (B), respectively. Figure 6(A) (a) shows that the value of n becomes larger when the diameter of particle increases and the shear thickening becomes more severely at the same time. Meanwhile, the value of n in the table of figure 6(B) (b) increases with the volume fraction increasing, which accords with the experimental results that the shear thickening becomes more severely with the volume fraction increasing. Generally, the fitting results accord with experimental results, indicating that the degree of shear thickening is closely related to the volume fraction and the size of dispersed phase particles. These results indicate that the increase of the volume fraction and particle size in a certain degree contributes to a more severe shear thickening.

According to hydrocluster mechanism (figure 6(C)), particles naturally flow due to random collisions among them in equilibrium. As the shear rate increase, particles become organized in the flow, which lowers the viscosity of the dispersion, therefore shear thinning occurs. If the shear rate reaches a critical value, hydrodynamic interactions between particles dominate and lead the random dispersion of particles to spawn hydroclusters (figure 6(C), orange). Therefore, transient fluctuations in particle concentration occur and the viscosity of the dispersion increase abruptly, that is shear thickening [64–67]. Recently, the contact rheology model is also proposed to explain the shear thickening behavior. Denn *et al* indicated that at low shear rates hydrocluster mechanism

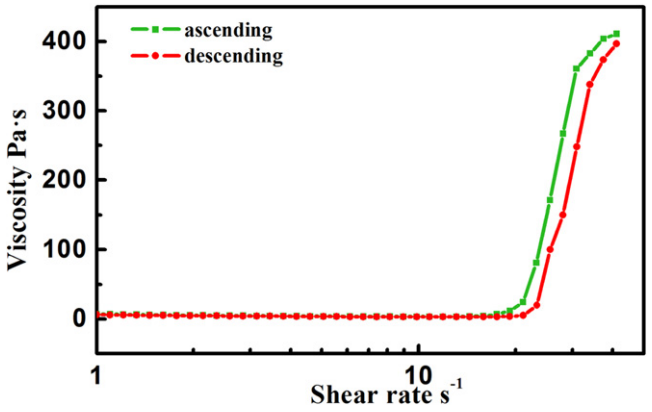

Figure 7. The reversible shear thickening behavior of the c-STF with a filling fraction of 59.1% (the average diameter of SiO_2 nanospheres is about 310 nm).

dominated the suspension due to the contactless state, while contact forces were essential for the shear thickening at high shear rates where the particles contacted each other [64].

Additionally, the reversibility of STF is an important property in practical applications. A good property of reversibility shows that the STF can resist impacts repeatedly. So we investigated the reproducibility of c-STF under cyclic loading. Figure 7 shows the viscosity of the c-STF with a filling fraction of 59.1% for both ascending and descending shear rate sweeps. There is a slight decrease in viscosity at a low shear rate and increases quickly as soon as the shear rate reaches the critical shear rate. The viscosity decreases immediately when the shear rate decreases. It should be noted that the viscosity is in good agreement at the same shear rate, which indicates that the shear thickening behavior of c-STF is well reversible.

Due to the c-STF is semitransparent, we observe the transition response from fluid state to solid state of the STF when subjected sudden impact via high-speed video camera. The initial state of c-STF is semitransparent blue fluid (figure 8(a)) and large amount of white solid material appear under the tip along with the glass bar when pulled out with a fast speed (b), (c). At the transient of the pulling out of glass bar from the c-STF, a fracture surface often observed in solid materials (d). The appearance of white solid material might due to a great deal of SiO_2 nanospheres gathering when the fluid subjected external impact. A great deal of SiO_2 nanospheres gathering leads the instant changes from initial fluid state to solid state of the inner structure of the c-STF and the color also changes to white. However, there is no apparent state and color change when the external impact is gentle (e)–(h). From the photographs (i)–(l), we can observe that the glass bar hardly inserts into c-STF when the glass bar suddenly plunges into the c-STF with a relatively fast speed and a little of white material is formed at the tip of the glass bar, which indicates that the viscosity of the c-STF increases abruptly and some of the fluid transforms into solid state when subjected suddenly impacts. In conclusion, the directly observation of the fluid state to solid state transition response

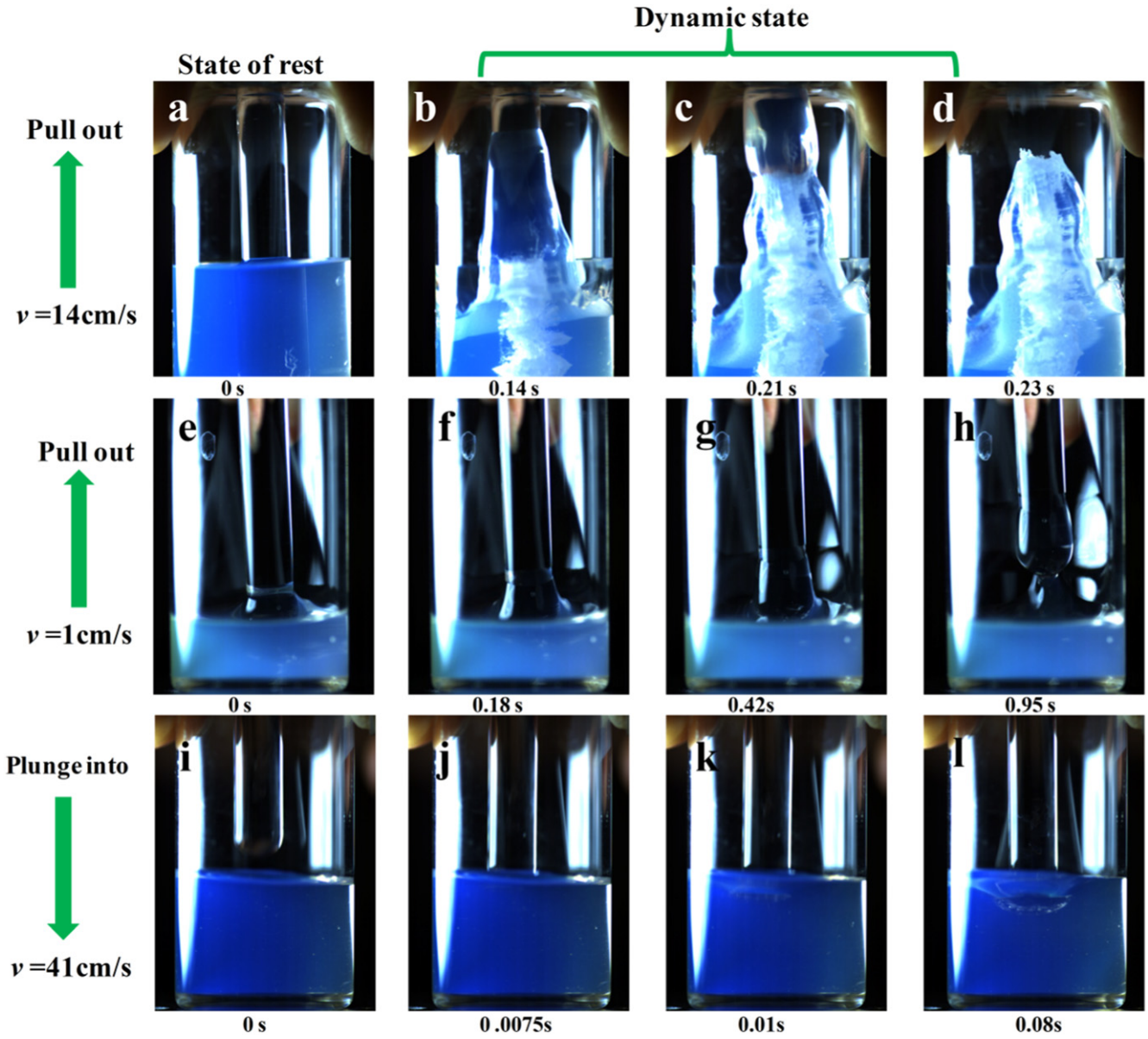

Figure 8. Photographs of the transition from fluid state to solid state in the shear thickening transient of the c-STF when it is subjected impacts with different rates. The photographs are taken when the glass bar is pulled out from the c-STF using fast speed (a)–(d) and low speed (e)–(h). The photographs (i)–(l) are taken when the glass bar suddenly plunges into the c-STF with a relatively fast speed.

in c-STF support a new way to study the shear thickening mechanism.

3.3. The effects of temperature on rheological properties of c-STF

It is reported that rheological properties of fluid materials are often temperature-dependent [68]. It is necessary to study the rheological properties of c-STF under different temperatures. The photographs in figure 9(a) show the color changes of c-STF along with temperature. The average diameter of SiO_2 nanospheres is about 200 nm. Due to the refractive index of PEG 200 changes with temperature [69, 70]. The refractive index of PEG 200 increases with the temperature decreasing. According to the equations of (1) and (2), the n_{eff} increases when the temperature decreases. So the wavelength of the center position of the reflection peak (λ) will become larger with the temperature decreasing and the λ will become smaller with the temperature increasing. The color of c-STF is blue-green at 25 °C and the color will exhibit blue shift and red shift when the temperature rising and decreasing separately, which accords with the theoretical explanation. For example, when the temperature of 25 °C decreases to 15 °C, the blue-green STF becomes yellow. When the temperature of 25 °C increases to 65 °C, the blue-green STF becomes blue firstly and then purple. Especially, the color of c-STF becomes muddy when the temperature increases to 75 °C, which may be explained that the structure of quasi-armorphous is destroyed at higher temperature. However, the color of c-STF becomes blue-green quickly when the temperature returns to room temperature, which shows that the color of c-STF has excellent reversibility. If the temperature is kept as

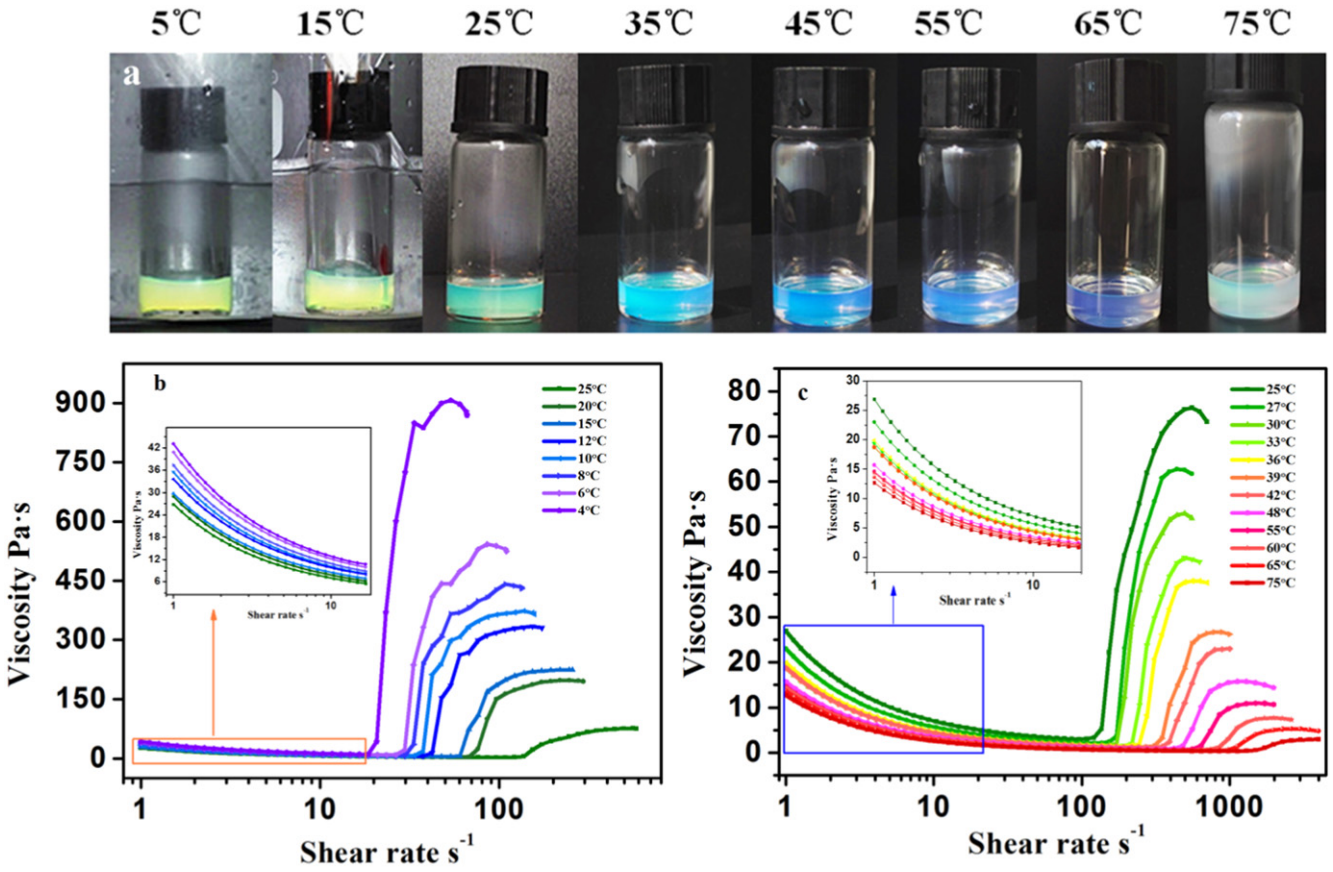

Figure 9. Photographs of the color changes in c-STF (the average diameter of SiO_2 nanospheres is about 200 nm) with the temperature changing (a). Viscosity versus shear rate for c-STF (the average diameter of SiO_2 nanospheres is about 200 nm) at the volume fraction of 58% when changing the temperature from 25 °C to 4 °C (b) and from 25 °C to 75 °C (c).

a constant, the changed color will keep for a long time. Additionally, the STF is a kind of colloid suspension, under steady state the nanoparticles will settle as time goes on, the time is about one month in our observation.

Additionally, we further study the rheological properties of c-STF along with temperature variations. Figures 9(b) and (c) show the static rheological properties c-STF. Curves of viscosity versus shear rate for all temperatures follow the same trend, which the viscosity decreases firstly (shear thinning) and then increases dramatically (shear thickening).

As for figures 9(b) and (c), we can observe that reducing the temperature of c-STF has four effects on the static rheological properties. First, the oligomeric liquid of PEG 200 generally increases its viscosity when lowering the temperature [58] and the inset of figure 9(b) clearly indicates that the initial viscosities increase as the temperature decreases. The initial viscosities increase from 26.9 Pa s to 43.1 Pa s when the temperature decrease from 25 °C to 4 °C. Second, the critical shear rates decrease from 136.8 s^{-1} to 18.7 s^{-1}. Third, the viscosity increase more rapidly following the critical shear rate, which shows that the steepness of the shear thickening region increases. Last, the overall increase in the magnitude of viscosity following the critical shear rate increases as temperature decrease. For example, the viscosity at the critical shear rate for 25 °C is 5.3 Pa s and rises to a maximum value, 76.3 Pa s (14.4 times), while the increase of viscosity is approximately 11.2 Pa s–907.2 Pa s (81 times) at 4 °C. Figure 9(c) shows the viscosity versus shear rate curves for the same c-STF over a temperature range of 25 °C–75 °C. The effects of temperature on the static rheological properties are similar to figure 9(b). The inset of figure 9(c) shows the details of the blue rectangle. The viscosity of the oligomeric liquid of PEG 200 decreases when the temperature increases. The initial viscosity and the degree of shear thickening of c-STF also decrease along with the temperature increasing. Generally, the color and rheological properties of c-STF is temperature-dependent, which means that c-STFs with specific color and rheological properties can be obtained from changing the temperature.

4. Conclusions

We develop a novel condensed colloidal fluid with both tunable non-iridescent structural colors and superior shear thickening rheological properties. The color of the photonic colloid fluid material can be controlled by changing the particle size, the volume fraction and temperature. The coloring mechanism of the quasi-amorphous photonic materials is discussed by 'tight bonding model'. This is a new candidate to investigate the mechanism of the structural color of quasi-photonic materials. It is the first time to develop novel STF

with rich structural color without using any pigments. The highlight of this work is studying the shear thickening mechanism of traditional STF by utilizing visual spectrum characterization and it is found that the shear thickening accompanied with the color transition. More *in situ* structural dependent light diffraction during the transition from fluid to solid state in shear thickening phenomenon is undergoing, which is important to study the mechanism through a visual optical method.

Acknowledgments

Financial supports from the National Natural Science Foundation of China (Grant Nos. 11772320). The Strategic Priority Research Program of the Chinese Academy of Sciences (Grant No. XDB22040502) is gratefully acknowledged. This work was also supported by Collaborative Innovation Center of Suzhou Nano Science and Technology.

ORCID iDs

Xinglong Gong https://orcid.org/0000-0001-6997-9526

References

[1] Brown E and Jaeger H M 2014 Shear thickening in concentrated suspensions: phenomenology, mechanisms and relations to jamming *Rep. Prog. Phys.* **77** 046602
[2] Hoffman R L 1972 Discontinuous and dilatant viscosity behavior in concentrated suspensions: I. Observation of a flow instability *Trans. Soc. Rheol.* **16** 155–73
[3] Hoffman R L 1974 Discontinuous and dilatant viscosity behavior in concentrated suspensions: II. Theory and experimental tests *J. Colloid Interface Sci.* **46** 491–506
[4] Barnes H A 1989 Shear-thickening ('dilatancy') in suspensions of nonaggregating solid particles dispersed in newtonian liquids *J. Rheol.* **33** 329–66
[5] Zhang X Z, Li W H and Gong X L 2008 The rheology of shear thickening fluid (STF) and the dynamic performance of an STF-filled damper *Smart Mater. Struct.* **17** 035027
[6] Kang T J, Kim C Y and Hong K H 2012 Rheological behavior of concentrated silica suspension and its application to soft armor *J. Appl. Polym. Sci.* **124** 1534–41
[7] Haris A, Goh B W Y, Tay T E, Lee H P, Rammohan A V and Tan V B C 2017 On the effectiveness of incorporating shear thickening fluid with fumed silica particles in hip protectors *Smart Mater. Struct.* **27** 015021
[8] Wei M, Hu G, Jin L, Lin K and Zou D 2016 Forced vibration of a shear thickening fluid sandwich beam *Smart Mater. Struct.* **25** 055041
[9] Tian T and Nakano M 2017 Design and testing of a rotational brake with shear thickening fluids *Smart Mater. Struct.* **26** 035038
[10] Gürgen S and Kuşhan M C 2017 The effect of silicon carbide additives on the stab resistance of shear thickening fluid treated fabrics *Mech. Adv. Mater. Struct.* **24** 1381–90
[11] Laha A and Majumdar A 2016 Shear thickening fluids using silica-halloysite nanotubes to improve the impact resistance of p-aramid fabrics *Appl. Clay Sci.* **132** 468–74
[12] Gürgen S and Kuşhan M C 2017 The stab resistance of fabrics impregnated with shear thickening fluids including various particle size of additives *Composites* A **94** 50–60
[13] Gürgen S and Kuşhan M C 2017 The ballistic performance of aramid based fabrics impregnated with multi-phase shear thickening fluids *Polym. Test.* **64** 296–306
[14] Yang W, Wu Y, Pei X, Zhou F and Xue Q 2017 Contribution of surface chemistry to the shear thickening of silica nanoparticle suspensions *Langmuir* **33** 1037–42
[15] Zheng S B, Xuan S H, Jiang W Q and Gong X L 2015 High performance shear thickening fluid based on calcinated colloidal silica microspheres *Smart Mater. Struct.* **24** 085033
[16] Yang H G, Li C Z, Gu H C and Fang T N 2001 Rheological behavior of titanium dioxide suspensions *J. Colloid Interface Sci.* **236** 96–103
[17] Zupančič A and Lapasin R 1997 Rheological characterisation of shear thickening TiO_2 suspensions in low molecular polymer solution *Prog. Org. Coat.* **30** 67–78
[18] Egres R G and Wagner N J 2005 The rheology and microstructure of acicular precipitated calcium carbonate colloidal suspensions through the shear thickening transition *J. Rheol.* **49** 719–46
[19] Yang H L, Ruan J M, Zou J P, Wu Q M, Zhou Z C and Xie Y Y 2009 Non-linear viscoelastic rheological properties of PCC/PEG suspensions *Chin. J. Chem. Phys.* **22** 46–50
[20] Zhang L M, Ma T, Yang J L and Huang Y 2004 Rheological behavior of alumina suspensions *J. Inorg. Mater.* **19** 1145–50
[21] Zupančič A, Lapasin R and Torriano G 1997 Rheological properties of $TiO_2/BaSO_4$ suspensions in oscillatory and steady shear flow *Prog. Org. Coat.* **30** 79–88
[22] Frith W J and Lips A 1995 The rheology of concentrated suspensions of deformable particles *Adv. Colloid Interface Sci.* **61** 161–89
[23] Jiang W, Sun Y, Xu Y, Peng C, Gong X and Zhang Z 2010 Shear-thickening behavior of polymethylmethacrylate particles suspensions in glycerine–water mixtures *Rheol. Acta* **49** 1157–63
[24] Chang L, Friedrich K, Schlarb A K, Tanner R and Ye L 2011 Shear-thickening behavior of concentrated polymer dispersions under steady and oscillatory shear *J. Mater. Sci.* **46** 339–46
[25] Otsubo Y, Fujiwara M, Kouno M and Edamura K 2007 Shear-thickening flow of suspensions of carbon nanofibers in aqueous PVA solution *Rheol. Acta* **46** 905–12
[26] Gürgen S, Kuşhan M C and Li W 2017 Shear thickening fluids in protective applications: a review *Prog. Polym. Sci.* **75** 48–72
[27] Gürgen S, Kuşhan M C and Li W 2016 The effect of carbide particle additives on rheology of shear thickening fluids *Korea-Aust. Rheol. J.* **28** 121–8
[28] Hasanzadeh M and Mottaghitalab V 2016 Tuning of the rheological properties of concentrated silica suspensions using carbon nanotubes *Rheol. Acta* **55** 759–66
[29] Hoffman R L 1982 Discontinuous and dilatant viscosity behavior in concentrated suspensions: III. Necessary conditions for their occurrence in viscometric flows *Adv. Colloid Interface Sci.* **17** 161–84
[30] Brown E and Jaeger H M 2012 The role of dilation and confining stresses in shear thickening of dense suspensions *J. Rheol.* **56** 875–923
[31] Brady J F and Bossis G 1985 The rheology of concentrated suspensions of spheres in simple shear flow by numerical simulation *J. Fluid Mech.* **155** 105–29
[32] Laun H M, Bung R, Hess S, Loose W, Hess O, Hahn K, Hadicke E, Hingmann R, Schmidt F and Lindner P 1992 Rheological and small angle neutron scattering investigation of shear-induced particle structures of concentrated polymer

dispersions unpublished to plane poiseuille and Couette flow a *J. Rheol.* **36** 743–87
[33] Newstein M C, Wang H, Balsara N P, Lefebvre A A, Shnidman Y, Watanabe H, Osaki K, Shikata T, Niwa H and Morishima Y 1999 Microstructural changes in a colloidal liquid in the shear thinning and shear thickening regimes *J. Chem. Phys.* **111** 4827–38
[34] Bender J W and Wagner N J 1995 Optical measurement of the contributions of colloidal forces to the rheology of concentrated suspensions *J. Colloid Interface Sci.* **172** 171–84
[35] Cheng X, McCoy J H, Israelachvili J N and Cohen I 2011 Imaging the microscopic structure of shear thinning and thickening colloidal suspensions *Science* **333** 1276–9
[36] Waitukaitis S R and Jaeger H M 2012 Impact-activated solidification of dense suspensions via dynamic jamming fronts *Nature* **487** 205–9
[37] Jiang W, Gong X, Xuan S, Jiang W, Ye F, Li X and Liu T 2013 Stress pulse attenuation in shear thickening fluid *Appl. Phys. Lett.* **102** 101901
[38] Han E, Peters I R and Jaeger H M 2016 High-speed ultrasound imaging in dense suspensions reveals impact-activated solidification due to dynamic shear jamming *Nat. Commun.* **7** 12243
[39] Peters I R, Majumdar S and Jaeger H M 2016 Direct observation of dynamic shear jamming in dense suspensions *Nature* **532** 214
[40] Yablonovitch E 1987 Inhibited spontaneous emission in solid-state physics and electronics *Phys. Rev. Lett.* **58** 2059
[41] Blanco A *et al* 2000 Large-scale synthesis of a silicon photonic crystal with a complete three-dimensional bandgap near 1.5 micrometres *Nature* **405** 437–40
[42] Froufe-Pérez L S, Engel M, Damasceno P F, Muller N, Haberko J, Glotzer S C and Scheffold F 2016 Role of short-range order and hyperuniformity in the formation of band gaps in disordered photonic materials *Phys. Rev. Lett.* **117** 053902
[43] Conley G M, Burresi M, Pratesi F, Vynck K and Wiersma D S 2014 Light transport and localization in two-dimensional correlated disorder *Phys. Rev. Lett.* **112** 143901
[44] Liew S F, Yang J K, Noh H, Schreck C F, Dufresne E R, O'Hern C S and Cao H 2011 Photonic band gaps in three-dimensional network structures with short-range order *Phys. Rev.* A **84** 063818
[45] Edagawa K, Kanoko S and Notomi M 2008 Photonic amorphous diamond structure with a 3D photonic band gap *Phys. Rev. Lett.* **100** 013901
[46] GarcÃ A P D, Sapienza R and Pez C L Ã 2010 Photonic glasses: a step beyond white paint *Adv. Mater.* **22** 12–9
[47] Ueno K, Inaba A, Sano Y, Kondoh M and Watanabe M 2009 A soft glassy colloidal array in ionic liquid, which exhibits homogeneous, non-brilliant and angle-independent structural colours *Chem. Commun.* **24** 3603–5
[48] Noh H, Liew S F, Saranathan V, Mochrie S G, Prum R O, Dufresne E R and Cao H 2010 How noniridescent colors are generated by quasi-ordered structures of bird feathers *Adv. Mater.* **22** 2871–80
[49] Forster J D *et al* 2010 Biomimetic isotropic nanostructures for structural coloration *Adv. Mater.* **22** 2939–44
[50] Dong B Q, Liu X H, Zhan T R, Jiang L P and Yin H W 2010 Structural coloration and photonic pseudogap in natural random close-packing photonic structures *Opt. Express* **18** 14430–8
[51] Ohtsuka Y, Seki T and Takeoka Y 2015 Thermally tunable hydrogels displaying angle-independent structural colors *Angew. Chem., Int. Ed.* **127** 15588–93
[52] Takeoka Y, Honda M, Seki T, Ishii M and Nakamura H 2009 Structural colored liquid membrane without angle dependence *ACS Appl. Mater. Interfaces* **1** 982–6
[53] Honda M, Seki T and Takeoka Y 2009 Dual tuning of the photonic band-gap structure in soft photonic crystals *Adv. Mater.* **21** 1801–4
[54] Arsenault A C, Puzzo D P, Manners I and Ozin G A 2007 Photonic-crystal full-colour displays *Nat. Photon.* **1** 468–72
[55] Stöber W, Fink A and Bohn E 1968 Controlled growth of monodisperse silica spheres in the micron size range *J. Colloid Interface Sci.* **26** 62–9
[56] Bogush G H, Tracy M A and Zukoski Iv C F 1988 Preparation of monodisperse silica particles: control of size and mass fraction *J. Non-Cryst. Solids* **104** 95–106
[57] Jin C, Meng X, Cheng B, Li Z and Zhang D 2001 Photonic gap in amorphous photonic materials *Phys. Rev.* B **63** 195107
[58] Hu Z, Lu X and Gao J 2001 Hydrogel opals *Adv. Mater.* **13** 1708–12
[59] Gao J and Hu Z 2002 Optical properties of N-isopropylacrylamide microgel spheres in water *Langmuir* **18** 1360–7
[60] Zhang Z, Yu K, Liao N, Yin H, Lou L, Yu Q, Liao Y and Zhu Z 2011 Fabrication of ZnO photonic amorphous diamond nanostructure from parrot feathers for modulated photoluminescence properties *Nanoscale* **3** 5000–6
[61] Doucet S M and Meadows M G 2009 Iridescence: a functional perspective *J. R. Soc. Interface* **6** (suppl. 2) 115–32
[62] Lidorikis E N E E, Sigalas M M, Economou E N and Soukoulis C M 1998 Tight-binding parametrization for photonic band gap materials *Phys. Rev. Lett.* **81** 1405
[63] Miyazaki H and Jimba Y 2000 *Ab initio* tight-binding description of morphology-dependent resonance in a bisphere *Phys. Rev.* B **62** 7976
[64] Gürgen S, Li W and Kuşhan M C 2016 The rheology of shear thickening fluids with various ceramic particle additives *Mater. Des.* **104** 312–9
[65] Mari R, Seto R, Morris J F and Denn M M 2014 Shear thickening, frictionless and frictional rheologies in non-Brownian suspensions *J. Rheol.* **58** 1693–724
[66] Lin N Y C, Guy B M, Hermes M, Ness C, Sun J, Poon W C K and Cohen I 2015 Hydrodynamic and contact contributions to continuous shear thickening in colloidal suspensions *Phys. Rev. Lett.* **115** 228304
[67] Seto R, Mari R, Morris J F and Denn M M 2013 Discontinuous shear thickening of frictional hard-sphere suspensions *Phys. Rev. Lett.* **111** 218301
[68] Warren J, Offenberger S, Toghiani H, Pittman C U Jr, Lacy T E and Kundu S 2015 Effect of temperature on the shear-thickening behavior of fumed silica suspensions *ACS Appl. Mater. Interfaces* **7** 18650–61
[69] Ottani S, Vitalini D, Comelli F and Castellari C 2002 Densities, viscosities, and refractive indices of poly (ethylene glycol) 200 and 400 + cyclic ethers at 303.15 K *J. Chem. Eng. Data* **47** 1197–204
[70] Yasmin M and Gupta M 2011 Density, viscosity, velocity and refractive index of binary mixtures of poly (Ethylene Glycol) 200 with ethanolamine, m-Cresol and aniline at 298.15 K *J. Solut. Chem.* **40** 1458–72